CR-332-761-001

DIRECT MEASUREMENT OF COMPRESSIBLE, TURBULENT BOUNDARY LAYER SKIN FRICTION ON A POROUS FLAT PLATE WITH MASS INJECTION

FINAL REPORT

JULY 1966

H. DERSHIN
C. A. LEONARD
W. H. GALLAHER
J. P. PALMER

Contract NAS 7-294

GENERAL DYNAMICS
Pomona Division

ACKNOWLEDGEMENT

The authors would like to thank Mr. W. A. Smith of the Convair Division of General Dynamics for operating the wind tunnel and Mr. E. R. Bartle of the Convair Division for his consultation efforts. The authors are also indebted to Mr. C. C. Pappas of Ames Research Center for the interest he displayed and for the valuable advice he contributed throughout the program.

CONTENTS

ILLUSTRATIONS

TABLES

Section 1

SUMMARY

An experimental investigation of skin friction on a porous flat plate in supersonic, turbulent flow has been carried out. Useful data has been obtained at Mach number 3.2 (nominal) and at two Reynolds numbers of the order of 10^7. Measurements were made with a skin friction balance which permitted mass injection through its friction surface. The injectant gas was nitrogen.

The results of the experiments are in essential agreement with the theory of Rubesin as regards skin friction reduction with mass injection. In addition, correlation of the skin friction data with heat transfer measurements, conducted previously by Bartle and Leadon, tend to verify the "Reynolds analogy" between skin friction and heat transfer developed by Rubesin.

Author

Section 2
INTRODUCTION

Reduction of momentum and energy transfer between a fluid and a boundary surface by means of liquid or gaseous injection through the surface is by no means a new technique. Early experiments with "sweat cooling" of rocket nozzles date back to 1946 (reference 1). Measurements of skin friction in the presence of mass transfer were performed as early as 1954 (reference 2). Both types of measurements have continued to the present time (e. g., references 3 – 11).

Of the two types of measurement, heat transfer, being susceptible to direct evaluation at the wall, is generally the simpler. The main obstacle here is generally one of being able to control or evaluate all possible heat sources and sinks. On the other hand, most skin friction measurements, with the exception of reference 6, have been based on indirect evaluation through physical probing of the boundary layer with, e. g., pressure probes or hot wires. The difficulty with pressure probe measurements results from the fact that the finite size of the probe restricts the extent to which the wall can be approached. And, since surface injection distorts the velocity profile near the wall so that extrapolation is difficult, determination of surface shear from a "wall" velocity gradient is not the most desirable approach. An alternative to skin friction evaluation from wall profile data is to integrate the velocity and density data through the boundary layer to obtain a momentum thickness distribution over the test plate. Skin friction is then calculated from a momentum-integral relation. Most investigators use this relation without regard for the fluctuating components of the turbulent flow. However, Goodwin (reference 10) has shown that neglecting these terms may result in significant errors in the presence of mass transfer.

Hot wires are more accurate than pressure probes due to their small diameter. However, hot wires are overly sensitive to local jetting of injectant gas. In addition, use of this instrument is impractical when foreign gases are injected since injectant concentration profiles are required.

An alternate technique for skin friction measurement (reference 6) has involved the determination of total drag reduction on a porous cone with gaseous injection. The data of reference 6 showed considerable variation from theoretical predictions. Thus, an independent check is warranted.

The measurement technique employed in the experiments conducted under the present study is direct, once the zero blowing skin friction is established, and is based on the classical floating element approach. The main variation has been to design the element so as to permit mass transfer through the friction surface. Thus, the mass transfer distribution over the test plate is continuous and local surface shear force is evaluated directly.

The objectives of these experiments are twofold. First, it is desired to compare the experimental results with available theories in an attempt to evaluate the usefulness of these theories for predicting skin friction reduction. Second, it is desired to correlate the skin friction data with the previously conducted heat transfer measurements of Bartle and Leadon (reference 7) to evaluate the Reynolds-type analogies predicted by the various theories.

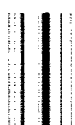

Section 3
NOMENCLATURE

A = area
C_f = local skin friction coefficient
C_F = average skin friction coefficient
c_p = specific heat at constant pressure
F = $(\rho v)_w/(\rho_\infty u_\infty)$
H = boundary layer form factor
M = Mach number
P = pressure
Pr = Prandtl number
Re = Reynolds number
St = Stanton number
T = temperature
u = stream velocity
v = injection velocity
$\dot{W}$ = flow rate
δ^* = displacement thickness
θ = momentum thickness
ϵ_H = turbulent eddy conductivity
ϵ_m = turbulent eddy viscosity
ρ = density

3.1 SUBSCRIPTS

o = stagnation, or zero blowing (in the case of C_f)
s = sublayer edge
w = wall
∞ = free stream

Section 4
DESCRIPTION OF EXPERIMENTAL FACILITIES

4.1 WIND TUNNEL

The experiments were conducted in the continuous operation wind tunnel at the Air Flow Facility of the Thermodynamics Laboratory of Convair Division of General Dynamics. Two sets of nozzle blocks were available producing Mach numbers of 2.0 and 3.2 (nominal) in the 3-1/2 x 6 inch rectangular test section.[1] Testing was conducted without heating of the air supply so that stagnation temperatures were in the range 100°F to 125°F.

4.2 MASS TRANSFER CELL AND TEST PLATE

A schematic of the porous flat plate model and plenum chamber (mass transfer cell) is shown in figure 1. It is identical to that used by Bartle and Leadon. The 5-1/2 x 16 inch flat porous plate was sintered from 5 microinch stainless steel powder. The solid wall ahead of the plate was ground to an 8 microinch finish. To achieve a uniform surface temperature, Bartle and Leadon constructed a compartmented plenum chamber with each compartment separately valved. Thus, the distribution of injectant could be varied along the surface of the plate and a uniform temperature maintained. This approach was followed in the experiments performed here to permit close correlation between the heat transfer and skin friction measurements.

The injectant distribution through the porous plate is set in the following manner. The mass flow through the skin friction balance is established. Then the other compartments are adjusted to give the desired mass flow profile along the plate centerline. The maximum mass flow is located at the first compartment. Therefore, the maximum valve setting of the first compartment becomes the upper limit.

Mass flow rate is measured with a hot wire anemometer. The anemometer is equipped with a guard section to average the mass flow over a small area. A sketch of the instrument is shown in figure 2.

In general, one surveys mass flow at approximately the midpoint of each compartment. A ratio between each compartment and the balance mass flow is compared with

---

[1] Experiments conducted at Mach number 2.0 were not successful. Mach waves generated by a slight curvature of the leading edge of the porous plate reflected from the top wall of the tunnel and intersected the friction balance. This is further explained in section 7.

the desired ratio. Once the proper compartment ratios are obtained, the average compartment mass flow is established. (The age and condition of the porous plate has resulted in non-uniform velocities in a few of the compartments.) Normally, five points are surveyed for each compartment. The average mass flow obtained generally agrees with the centerline value. Finally, a centerline survey at each 1/2 inch provides a smooth curve for an integration to determine the average mass flow. The ratio of the balance to the average mass flow is used later to calculate the balance mass flux parameter.

The total injectant flow to the porous plate is measured by a Fischer and Porter flowmeter and corrected for pressure and temperature. The flowmeter reading is given in percent and the corresponding flow at STP is obtained from the flowmeter calibration curve. The flow is corrected to pressure and temperature by the expression

$$(\dot{W}_{FM})_{P,T} = (\dot{W})_{STP} * \sqrt{\frac{P_{FM}\ (\text{in. Hg. A})}{30\ \text{in. Hg. A}} \quad \frac{530°F}{T_{FM}(°F)}} \tag{1}$$

The resulting flow is corrected to lb/sec and divided by the plate surface area to give the expression

$$(\rho V)_{Bal} = \left(\frac{\rho V_{Bal}}{\rho V_{total}}\right)\left[\frac{(\dot{W})_{P,T}}{A_{plate}}\right] \sim \frac{lbm}{ft^2 sec} \tag{2}$$

In this expression $(\rho V_{Bal}/\rho V_{total})$ is based on the mass flow survey.

A typical injection distribution is shown in figure 3, compared to the distribution of reference 7. Some degradation in porosity is observed near the leading edge of the plate. However, this is not taken to be significant since the center of the floating element is located roughly 11-1/4 inches downstream of the start of the porous section.

4.3 SKIN FRICTION BALANCE

The application of the floating element technique to the present investigation required the following considerations: (1) that the balance be designed for incorporation into the flat-plate wind tunnel model described in paragraph 4.2; (2) that the balance be properly located in the friction plate to avoid edge effects originating with the plate (while this was achieved at M = 3, at the lower Mach number edge originated problems did occur; these are explained in section 7); (3) that provisions be made for regulated injection of transpiration gas through the porous floating element; (4) that the gap between the floating element and the model plate be isolated from the flow of transpiration gas; (5) that the displacement monitoring be frictionless; and (6) that provisions be made for precise alignment of the floating element with respect to the model plate. (Problems associated with alignment are discussed in section 6.)

The resulting configuration is shown in figures 4A and 4B. The lettered references are identified below. The porous floating element (A) is bonded to the end of a small plenum chamber (B) with an asbestos filled epoxy resin. The porous disc is sintered 5 microinch stainless steel powder, 0.250 inch thick. The floating element is supported on three fixed-end flexure rods (C) which are held stationary at the lower ends with set-screws in separate rigid cylinders (D). These cylinders are brazed into the base ring (E). Injectant gas is conducted to the floating assembly through a flexible metal bellows (F), bonded at the top around a hole in the floating plenum (B). The bottom of the bellows is bonded to a 1/8-27 pipe fitting (G). A base leg (H) extending from the base plate secures the pipe fitting with an O-ring seal (I). Displacement of the floating element is monitored with a miniature differential transformer (J). The transformer core is supported by a bracket extending from the floating plenum, and the transformer coil assembly is supported by an adjustable bracket mounted on the base plate. The transformer leads are fed through a miniature connector potted into the base plate. Two thermocouples (K) are housed in the porous element and extend through the bellows. The friction surface of the floating element is centered in the downstream portion of the porous plate. The installation is shown in figure 5.

One of the major design problems involved the necessary reduction of the pressure gradient at the edge of the floating element due to the gap. Previous designers of floating element instruments, not concerned with mass transfer, reduced these effects by chamfering the edge of a circular floating element and by positioning it 0.001 inch below and parallel to the model surface. However, when provisions are included for gas injection through the floating element, the chamfer would disturb the continuity of the injected flow distribution. The alternative was to reduce the maximum flow-directed component of the gap such that it is much less than the main stream boundary layer thickness. In order to satisfy this condition and still obtain adequate stop-to-stop displacement for the floating element, the surface geometry shown in figure 6 was proposed. The maximum longitudinal component of the gap at the cusps (dimension B of figure 6) is 0.075 inch which results in a gap-width to boundary layer ratio of about 1:7. The minimum gap dimension (A) is roughly 0.0075 inch.

Additional interruption of the boundary layer at the gap due to passage of gas through the gap is eliminated by sealing the porous edges of the floating element and flat plate with an epoxy resin and by isolating the plenum region beneath the floating element from the compartment which houses the balance. This isolation is provided by the cylindrical wall, which is an integral part of the base plate in figure 4A and which seals at the bottom side of the porous plate with a molded elastomer. [2]

Displacement of the floating element is monitored with a Schaevitz miniature differential transformer using a Daytronic Type 61 readout device. The scale resolution is 0.00005 inch. The transformer core does not contact the coil assembly when the core is properly aligned; hence, the deflection is reversible.

---

[2] Injectant gas leakage through the gap did occur at times. However, this situation was easily identifiable by its influence on the static pressure distribution in the vicinity of the balance. Of course, no data was taken to be reliable under these conditions.

Vertical alignment of the balance includes simultaneous alignment of the floating element with respect to the model plate and of the transformer core with respect to the coil assembly. Since the transformer is inaccessible when the balance is completely assembled, the core must be aligned while the subassembly (including the floating element, flexure system, transformer, and bellows) is removed from the housing. Then the subassembly is installed and alignment of the floating element is obtained by adjusting the pressure on the O-rings adjacent to each of the three base legs and the base plate. If proper alignment cannot be obtained and it is necessary to move one or more flexure rods in the base legs by adjustment of the respective setscrews, it again becomes necessary to remove the subassembly to realign the transformer core. Then, when the balance subassembly is reinserted in the housing, the desired alignment is obtained by readjusting the O-ring pressure.

4.4 CALIBRATION

Calibrations were performed employing the specially designed fixture shown in figure 7. The fixture has a tee-shaped arm balanced on a knife-edge support. One side of the tee carries a pan to hold calibrated weights, and the other side holds a counterweight to balance the weight of the empty pan. A prong on the bottom of the tee contacts a block resting on the floating element. The lever ratios are such that the calibrated weight is equal to the horizontal force applied to the floating element. Calibration is obtained by dropping successive weights into the pan and observing the incremental deflections. The calibration is linear throughout the allowed displacement.

The effect of transpiration blowing is to slightly displace the zero-point of the floating element as a result of the tendency for the bellows to become straight when pressurized. The effect on the spring rate (slope of the calibration line) is also slight. Nevertheless these effects are always accounted for. Thus, each injection test point is separately calibrated. A typical calibration curve is shown in figure 8 over the range of blowing rates.

4.5 ASSOCIATE MEASUREMENTS

In addition to the basic skin friction measurements, instrumentation was provided to record wall temperature and static pressure, stagnation temperature, stagnation pressure, and injectant temperature. Further, a micrometer adjusted surface impact pressure probe (50 mils in diameter) could be located 1-1/2 inches upstream, downstream, or directly over the floating element to provide an independent check of the zero blowing skin friction measurement. As in reference 7, the performance curves of Fenter and Stalmach (reference 12) were used to evaluate the zero blowing skin friction from the impact pressure measurement.

Section 5
ZERO INJECTION BOUNDARY LAYER CHARACTERISTICS

The measurements of Bartle and Leadon established that the boundary layer over the test plate was turbulent. This was verified during the present study.

The boundary layer was surveyed with a small (0.008 inch by 0.025 inch) pitot probe, and velocity and density profiles were computed. Profiles taken directly over the skin friction balance and 1-1/2 inches upstream and downstream of its center are shown in figure 9. (These were used in the calculation of the boundary layer shape parameter.)

Employing a Stewartson type coordinate transformation, Burke (reference 14) shows that the boundary layer shape parameter (δ^*/θ) is given by

$$\frac{\delta^*}{\theta} = \frac{T_o}{T_\infty}\left(1 + H_i \frac{T_w}{T_o}\right) \tag{3}$$

where H_i is the shape parameter in the transformed "incompressible" plane. For a (1/7) turbulent velocity profile in the incompressible plane, $H_i = 1.28$. Then, at Mach number 3.2 (δ^*/θ) as calculated from the above equation should be close to 6.6. Table 1 below lists the measured form factors. They are seen to be within 1 percent of each other and quite close to the form factor predicted by equation 3.

Table 1
MEASURED FORM FACTORS

Location	(δ^*/θ)
1-1/2 inch upstream	6.06
Over balance	6.04
1-1/2 inch downstream	6.00

For comparison, H_i for a laminar boundary layer in the "incompressible" plane is 2.5. This would lead to a compressible form factor, at the present test conditions, equal to about 10. Thus, the boundary layer is taken to be turbulent.

Similar measurements were not taken at Mach number 2 for the reasons indicated in section 7.

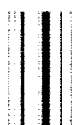

Section 6
VERTICAL POSITIONING

Proper vertical positioning of the balance with respect to the surrounding plate is, without question, the most critical ground rule of the experiments. For example, table 2 shows a typical variation in C_{f_o} measurements with vertical displacement.

Table 2
VARIATIONS IN C_{f_o}

Approximate Vertical Displacement	C_{f_o} Error
-0.002 inch	-20%
-0.0015 inch	-10%
+0.001 inch	+20%

The basis for these variations may, possibly, be explained in the following manner: With the balance below the plate surface a net adverse pressure gradient may occur over the instrument. This would result in a decreased C_{f_o}. With the balance above the plate, the measurement now includes the total drag. That is, both the dynamic pressure and a balance base drag add to the balance skin friction to give an erroneously high deflection.

The situation is further complicated by mass injection, particularly when the balance position is high. Injection distorts the upstream velocity gradient, reducing the dynamic pressure on the balance. Injection also simulates "base bleed," thus reducing the "base" drag of the instrument. The result is a relatively large decrease in total drag or, if not interpreted correctly, what appears to be a large reduction in "skin friction" as a result of the mass injection. At high injection rates, this trend is reversed. Drag reduction ceases and, in fact, begins to increase with mass injection. The reason for this is not clear. However, it indicates a net positive pressure gradient either over or within the balance assembly. Thus, data taken with the balance located high, with respect to the plate, is not usable since the non-friction drag components vary with injection, and therefore, cannot be linearly subtracted from a total drag measurement.

As a result of the above considerations, a significant part of each experimental run involved the determination of the proper balance setting. This was achieved by comparing the zero blowing measurement with that recorded by the impact pressure probe.

The balance would then be adjusted until both readings matched within a few percent. Following proper zero positioning, the balance would be recalibrated and the zero reading checked again. In most cases, it was found that a balance position roughly 0.0005 inch below the test plate surface resulted in the best correlation between the probe and balance measurements for zero blowing and in a smoothly varying and repeatable skin friction variation with mass injection.

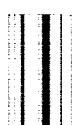

Section 7
PRESENTATION OF DATA

Skin friction data were acquired in the following manner. After stabilization of the wind tunnel conditions, the proper vertical positioning was determined. Then, nitrogen gas was metered into the mass transfer cell. The injectant gas was slightly warmed to keep the plate temperature relatively constant (close to the zero blowing adiabatic wall temperature) throughout the tests. Balance deflection was read directly from the Daytronic unit and converted to shear force via the calibration curve. The shear force was then divided by the balance area and by the stream dynamic pressure to obtain a skin friction coefficient.

Figure 10 shows the basic data taken at Mach number 3.18 and at a stagnation pressure level of 110 in. HgA. This corresponds to a Reynolds number, based on the 33 inch distance from the nozzle throat, of about 1.9×10^7. The different symbols indicate separate tests. Repeatability appears to be within a few percent.

For these test conditions, the momentum thickness Reynolds number is about 33,400. From the analysis of Deissler and Loeffler (reference 17), this would lead to a zero blowing skin friction coefficient of about 0.0011. The zero blowing skin friction coefficient as measured by the balance was about 0.0009; lower than the theoretical prediction. Nevertheless, it is consistent with the previous measurements of Bartle and Leadon and the present impact probe measurements.

Figure 11 shows the data plotted as C_f/C_{f_o} versus $2F/C_{f_o}$. The theoretical predictions of Rubesin (reference 13) are shown in the same figure. Correlation appears to be excellent.

Figure 12 shows the basic data taken at Mach number 3.18 and a stagnation pressure level of 220 in. HgA, superimposed on the 110 in. HgA data. Here, significant balance vibration occurred for zero blowing, as indicated in the figure[1]. The data were therefore reduced to C_f/C_{f_o} plots in two ways. First C_{f_o} was determined by extrapolating the skin friction data to zero blowing (a familiar technique for heat transfer measurements). Secondly, C_{f_o} was taken to be that recorded by the impact probe. These data are shown in figure 13 together with the data taken at 110 in. HgA. The variation between the two sets of data is seen to be small. However, there appears to be a slight Reynolds number dependency, as predicted by Rubesin. This is more easily seen in figure 14 where C_f/C_{f_o} is plotted against $2F/C_f$ along with Rubesin's theoretical predictions for both Reynolds numbers.

---

[1] As soon as significant blowing was begun, however, balance vibration essentially ceased.

It was also intended that data be taken at Mach number 2.0. However, it was found that at Mach number 2.0 a Mach wave, generated by a mechanical distortion of the leading edge of the porous section, reflected from the upper wall of the tunnel and impinged on the exact location of the skin friction balance. Data taken under these conditions are not felt to be reliable and are therefore not presented.

A comparison of the Mach number 2.0 pressure distribution with the Mach number 3.2 pressure distribution is shown in figure 15 to illustrate the effect of the Mach wave. Also included are subsequent data taken at Mach number 2.0 on a new plate, purchased after the termination of the present study. Here, the leading edge effect is seen to be completely eliminated. However, program limitations prohibited installation of the friction balance in the new plate.

Section 8
EVALUATION OF REYNOLDS ANALOGY

Most theoretical evaluations of heat transfer in the presence of mass injection (see e.g., references 13, 14 and 16) evolve through (1) the determination of a basic skin friction law and, (2) the derivation of a relationship between skin friction and heat transfer (i.e., a Reynolds analogy for mass transfer). The resulting equation describing Reynolds analogy is usually of the following form (reference 15):

$$\frac{St}{C_f} = \frac{(2F/C_f)}{2\left\{(1+\frac{2F}{C_f})\,(1+\frac{2F}{C_f}\,\frac{u_s}{u_\infty})^{P_r-1}-1\right\}} \tag{4}$$

where a "turbulent" Prandtl number ($\epsilon_m c_p/\epsilon_H$) equal to unity has been assumed. Thus, considering ($2F/C_f$) a parameter in itself, the only other influencing factor on (St/C_f) is seen to be the velocity ratio at the edge of the laminar sublayer (u_s/u_∞). Dorrance (reference 15) treats both ($2F/C_f$) and (u_s/u_∞) parametrically and shows that any separate increase in either one increase (St/C_f). These effects are shown in figure 16, reproduced from reference 15. Thus, it is to be expected that unless a considerable reduction in (u_s/u_∞) occurs with mass injection, the Reynolds analogy parameter (St/C_f) should increase with increased mass injection. In fact, this trend is shown both by the analyses of references 13 and 16.

The calculation of (St/C_f) from the heat transfer data of Bartle and Leadon and the skin friction data of the present study is complicated by two factors. First, it was found to be impractical to perform skin friction measurements in a heated condition. This was due to the fact that differential thermal expansions within the skin friction balance caused the floating element to be non-flush with the plate surface. As pointed out in section 6, this results in measurements which are impossible to interpret. Secondly, although the skin friction measurements were conducted in the same mass transfer cell as were the heat transfer measurements of Bartle and Leadon, the latter were performed at the University of Southern California Engineering Center (as pointed out in reference 7) while the former were performed at the Convair Division of General Dynamics. It was found to be impossible to generate supersonic flow at the low stagnation pressures employed at USC-EC. Thus, the Reynolds numbers attained during the skin friction measurements were somewhat higher than those of the heat transfer tests.

According to Rubesin, the effect of Reynolds number variation on a correlation of St/St_o versus F/St_o is small.

According to Knuth and Dershin (reference 16), both heat transfer and skin friction may be correlated in a reference temperature plane by a single curve, regardless of Reynolds number.

The approach taken here is directed towards evaluation of both theories. The following steps are then taken:

1. Rubesin's Theory
   a. The St/St_o versus F/St_o data of Bartle and Leadon are scaled according to Rubesin's theory to correct for Reynolds number. This amounts to a maximum correction of about 10 percent at the highest blowing rates.
   b. The data are then multiplied through by a zero blowing Stanton number corresponding to the average adiabatic wall skin friction measurements. This leads to a smooth plot of St versus F.
   c. A smooth curve is drawn through the C_f/C_{f_o} versus $2F/C_{f_o}$ data. This is then converted to C_f versus F by multiplying through by the average measured C_{f_o}.
   d. The ratio St/C_f is then formed at particular values of F and plotted as St/C_f versus $2F/C_f$ so as to permit comparison with Rubesin's theory.

      The results of these calculations are shown in figure 17. The Reynolds analogy factor (St/C_f) is seen to follow the general trend predicted by Rubesin but is somewhat higher at the lower blowing rates.

2. Theory of Knuth and Dershin.

   The "universal" curve of reference 16 was based in part on the heat transfer data of Bartle and Leadon. Thus, the remaining step requires only that the skin friction data taken here be converted to the reference temperature plane and plotted against the "universal" curve. The resulting data are shown in figure 18. It is seen that the low Reynolds number data fall close to the desired curve; the higher Reynolds number data fall somewhat below the desired curve.

Section 9
COMPARISON WITH OTHER DATA SOURCES

Figure 19 shows the data taken during this investigation compared with the data of references 2, 6, 10, 11, 18, and 19. The data are seen to fall close to the low speed data of references 2, 6, 11, and 19 at the low blowing rates, and close to the low speed data of references 10 and 19 at the high blowing rates.

The Mach number dependence observed by Pappas and Okuno for supersonic flow over a porous cone has not been observed for the flat plate experiments performed here. While the reason for this difference is not perfectly clear, the following observation is offered.

It may be, that the values measured by the cone, include the effects of local pressure gradients. Examing a familiar integral form of the boundary layer momentum equation, it is seen that the local skin friction is influenced by pressure gradient through the last term shown below:

$$C_f = 2\left(\frac{d\theta}{dx} - F\right) - \frac{\theta}{q}\left[2 + \frac{\delta^*}{\theta} - M_e^2\right]\frac{dp}{dx} \qquad (5)$$

An accumalation of small, local positive pressure gradients on a cone could easily increase the skin friction over that anticipated for an "ideal" cone. Thus, it is suggested that the Mach number effect observed by Pappas and Okuno may only be apparent for total skin friction on a cone and may not be relevant for local flat plate skin friction.

Section 10
CONCLUSIONS

It has been established that the balance technique can be used to provide reliable skin friction data with mass injection. Correlation with theory shows that the method of Rubesin satisfactorily predicts the skin friction reduction with mass injection over the range of the test conditions. Rubesin's theory is also found to be somewhat better than the method of Knuth and Dershin for these test conditions.

Correlation with the heat transfer data of Bartle and Leadon shows that Rubesin's "Reynolds Analogy" is also accurate over the test conditions.

Section 11
REFERENCES

1. Dawes, P., Wheeler, H., "Preliminary Experiments on Sweat Cooling," JPL/CIT P.R. 3-13, July 1946.

2. Mickley, H.S., Ross, R.C., Squyers, A. L., Stewart, W.E., "Heat, Mass and Momentum Transfer for Flow over a Flat Plate with Blowing or Suction," NACA TN-3208, July 1954.

3. Scott, C. J., Anderson, G. E., Elgin, D. R., "Laminar, Transitional and Turbulent Mass Transfer Cooling Experiments at Mach Numbers of 3 to 5," University of Minnesota, Institute of Technology, Rosemount Aeronautical Laboratories, AFOSR TN-59-1305, August 1957.

4. Mickley, H. S., Davis, R. S., "Momentum Transfer for Flow Over a Flat Plate with Blowing," NACA TN-4017, November 1957.

5. Bartle, E. R., Leadon, B. M., "Experimental Evaluation of Heat Transfer with Transpiration Cooling in a Turbulent Boundary Layer at M = 3.2," Journal of the Aero/Space Sciences, Volume 27, No. 1, January 1960.

6. Pappas, C. C., Okuno, A. F., "Measurements of Skin Friction of the Compressible Turbulent Boundary Layer on a Cone with Foreign Gas Injection," Journal of the Aero/Space Sciences, Volume 27, No. 5, May 1960.

7. Bartle, E. R., Leadon, B. M., "The Effectiveness as a Universal Measure of Mass Transfer Cooling for a Turbulent Boundary Layer," Proceedings of the 1962 Heat Transfer and Fluid Mechanics Institute, Stanford University Press, Stanford, California, June 1962.

8. Danberg, J. E., "Characteristics of the Turbulent Boundary Layer With Heat and Mass Transfer at M = 6.7," United States Naval Ordnance Laboratory NOLTR 64-99, White Oak, Maryland, October 1964.

9. Pappas, C C., Okuno, A. F., "Measurement of Heat Transfer and Recovery Factor of a Compressible Turbulent Boundary Layer on a Sharp Cone With Foreign Gas Injection," NASA TN D-2230, April 1964.

10. Goodwin, B. M., "The Transpired Turbulent Boundary Layer With Zero Pressure Gradient," MIT Doctor of Science Thesis, May 1961.

11. Smith, K. A., "The Transpired Turbulent Boundary Layer," MIT Doctor of Science Thesis, May 1962.

12. Fenter, F. W., Stalmach, C. L., Jr., "The Measurement of Turbulent Boundary Layer Shear Stress by Means of Surface Impact-Pressure Probes," Journal of the Aero/Space Sciences, Volume 25, No. 12, December 1958.

13. Rubesin, M. W., "An Analytical Estimation of the Effect of Transpiration Cooling on the Heat Transfer and Skin Friction Characteristics of a Compressible, Turbulent Boundary Layer," NACA TN 3341, December 1954.

14. Burke, A. F., "Turbulent Boundary Layers on Highly Cooled Surfaces at High Mach Numbers," Proceedings of Symposium on Aerothermoelasticity, ASD Technical Report 64-645, October 1961.

15. Dorrance, W. H., Viscous Hypersonic Flow, McGraw-Hill Book Company, Inc., New York 1962.

16. Knuth, E. L., Dershin, H., "Use of Reference States in Predicting Transport Rates in High-Speed Turbulent Flows with Mass Transfers," International Journal of Heat and Mass Transfer, Volume 6 pp 999-1018.

17. Deissler, R. G., Loeffler, A. L. Jr., "Analysis of Turbulent Flow and Heat Transfer on a Flat Plate at High Mach Numbers With Variable Fluid Properties," NACA TN 4262, April 1958.

18. Tendeland, Thorval, and Okuno, Arthur F., "The Effect of Fluid Injection on the Compressible Turbulent Boundary Layer – the Effect on Skin Friction of Air Injected Into the Boundary Layer of a Cone at M = 2.7," NACA RM A56D05, 1956.

19. Kendall, R. M., Rubesin, M. W., Dahm, T. J., Mendenhall, M. R., "Mass, Momentum, and Heat Transfer Within a Turbulent Boundary Layer With Foreign Gas Mass Transfer at the Surface, " Vidya Report No. 111, February 1964, ASTIA AD 619209.

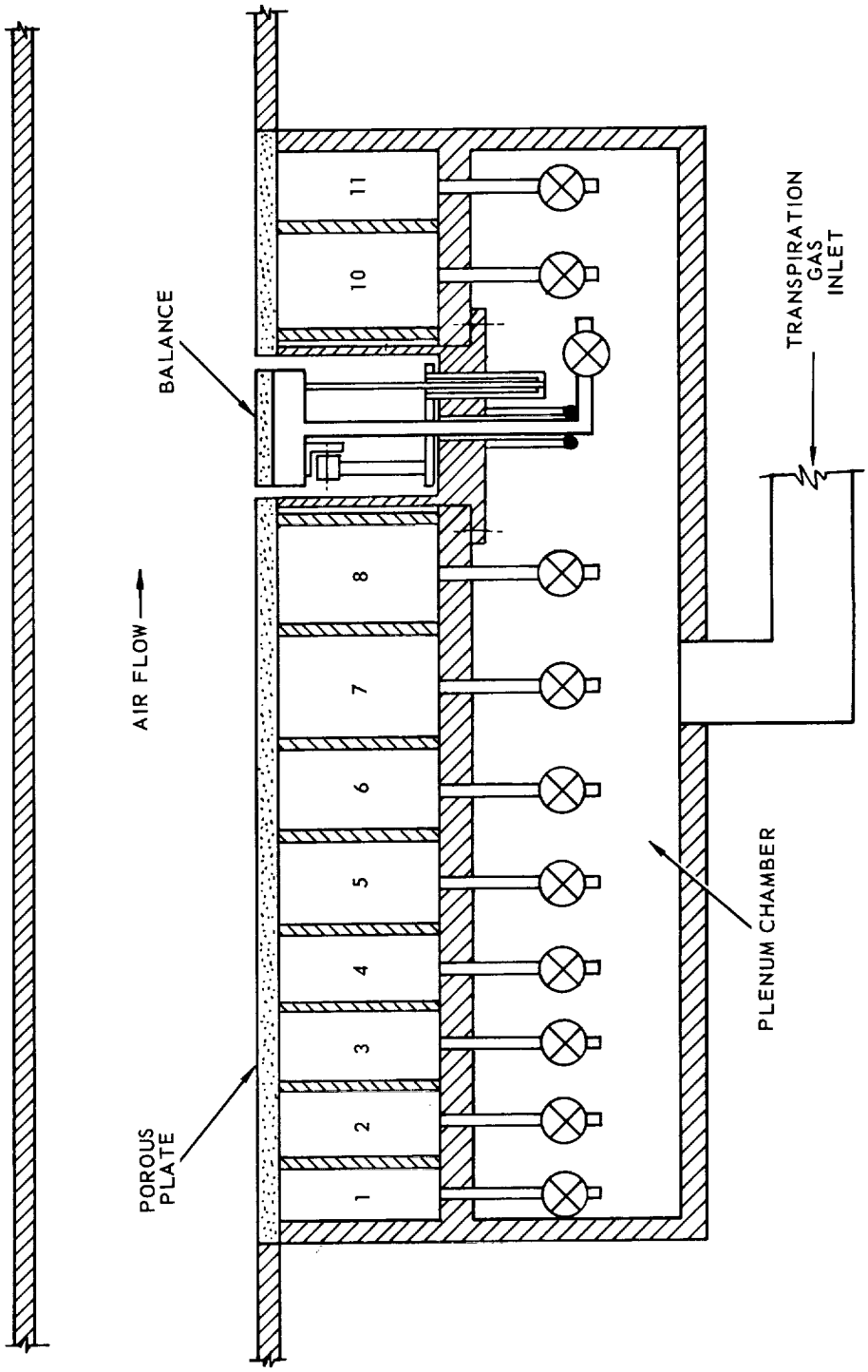

Figure 1. Test Section Schematic.

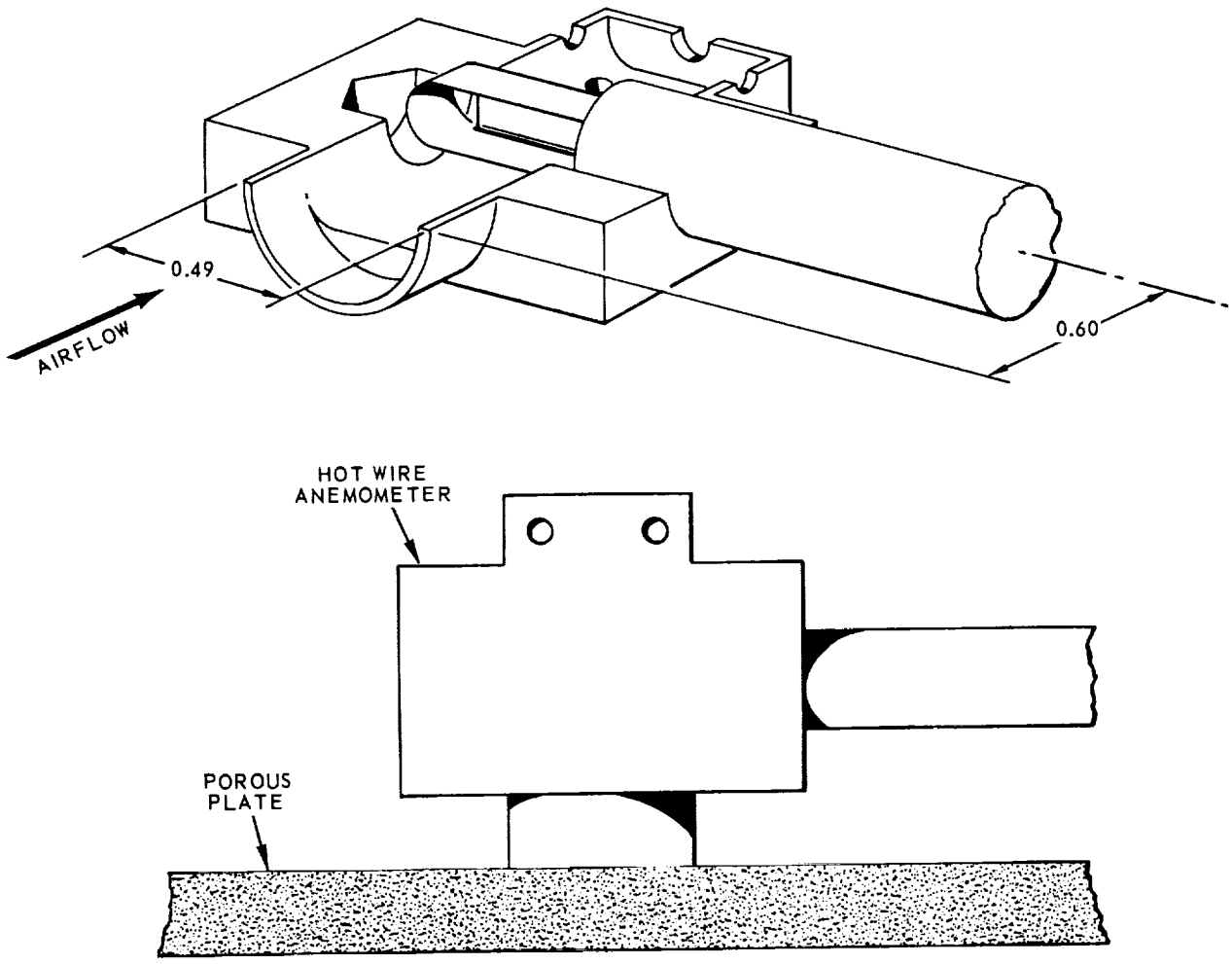

Figure 2. Hot Wire Anemometer With End Cap Sectioned.

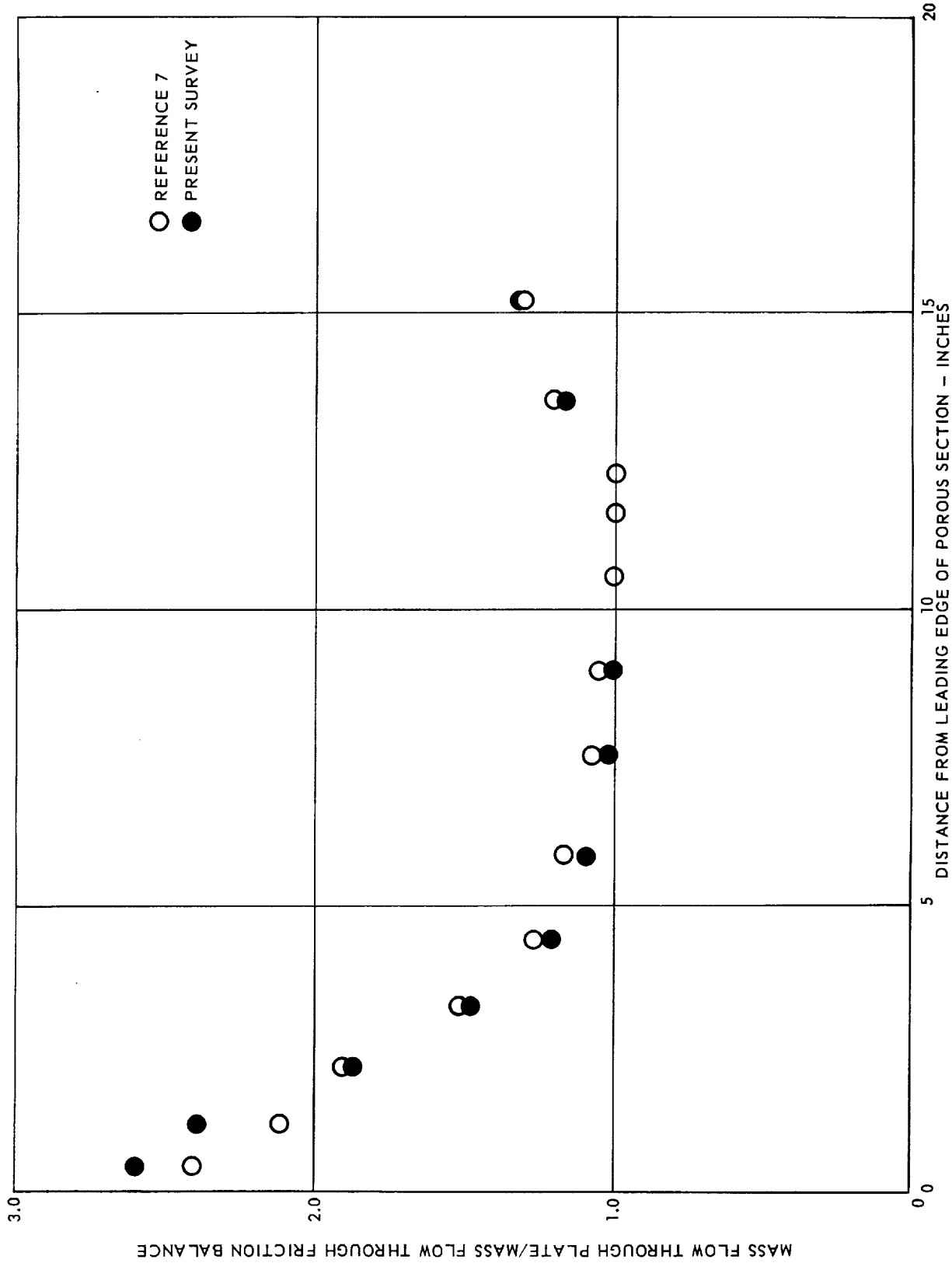

Figure 3. Injection Distribution for the Porous Plate.

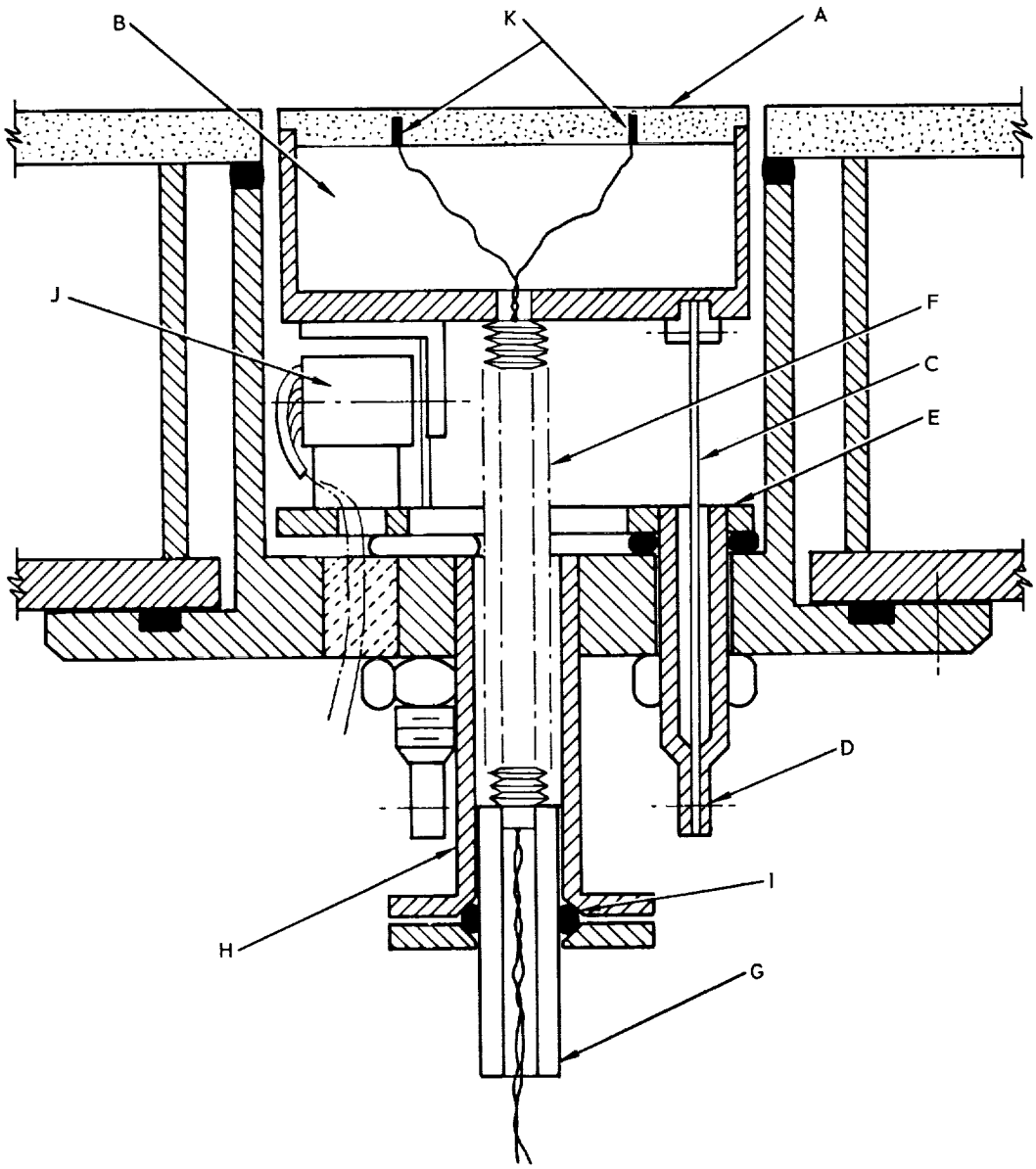

Figure 4A. Skin Friction Balance Schematic.

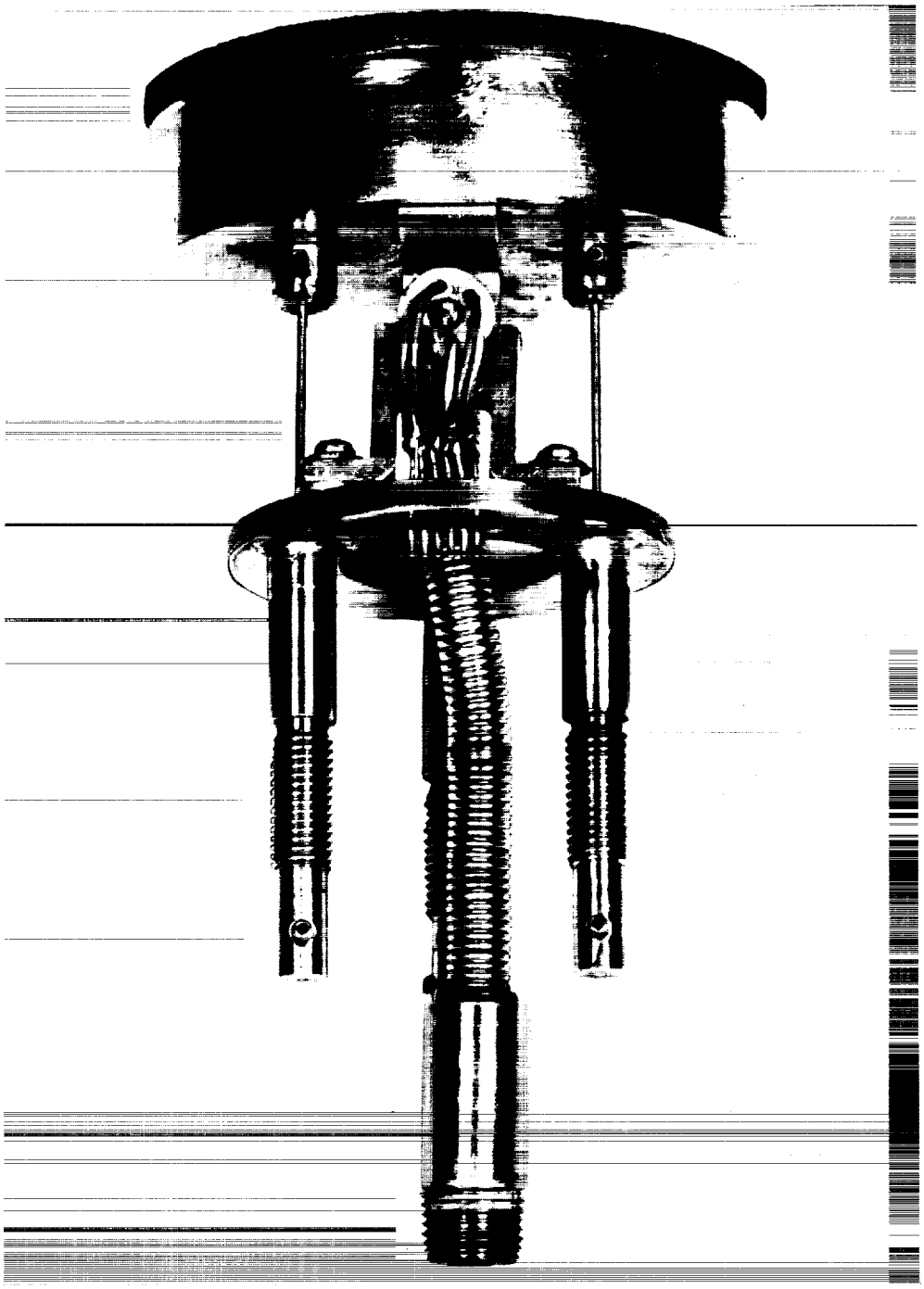

Figure 4B. Skin Friction Balance Floating Element.

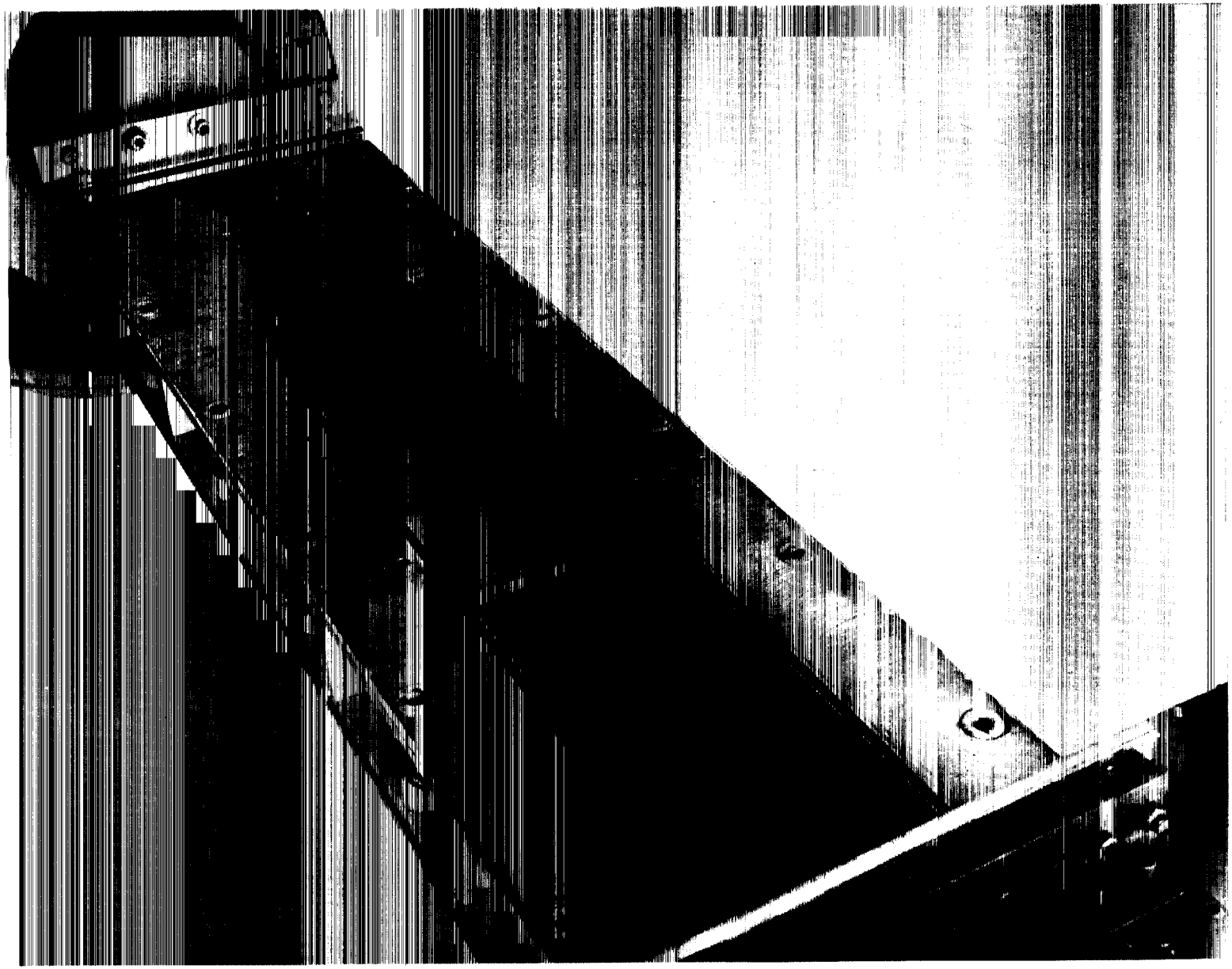

Figure 5. Direct Measuring Aerodynamic Skin Friction – Balance Installed in Wind Tunnel.

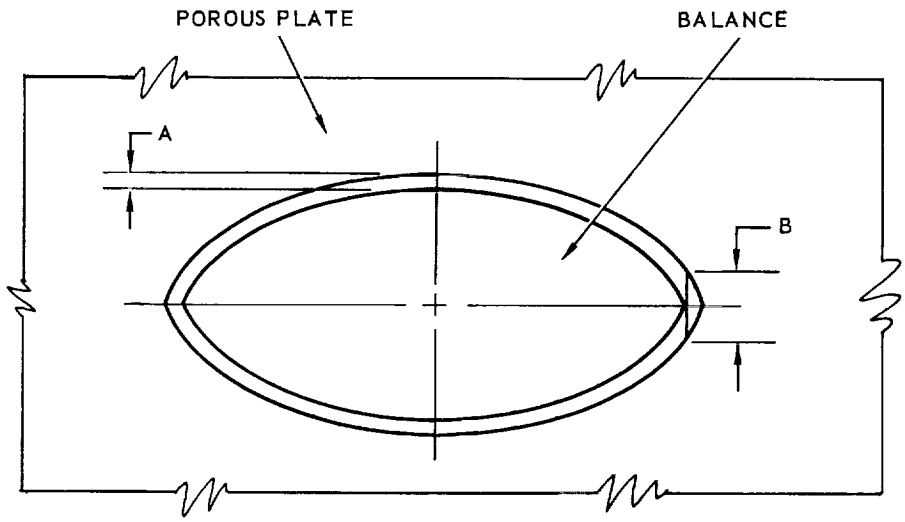

Figure 6. Friction Surface Schematic.

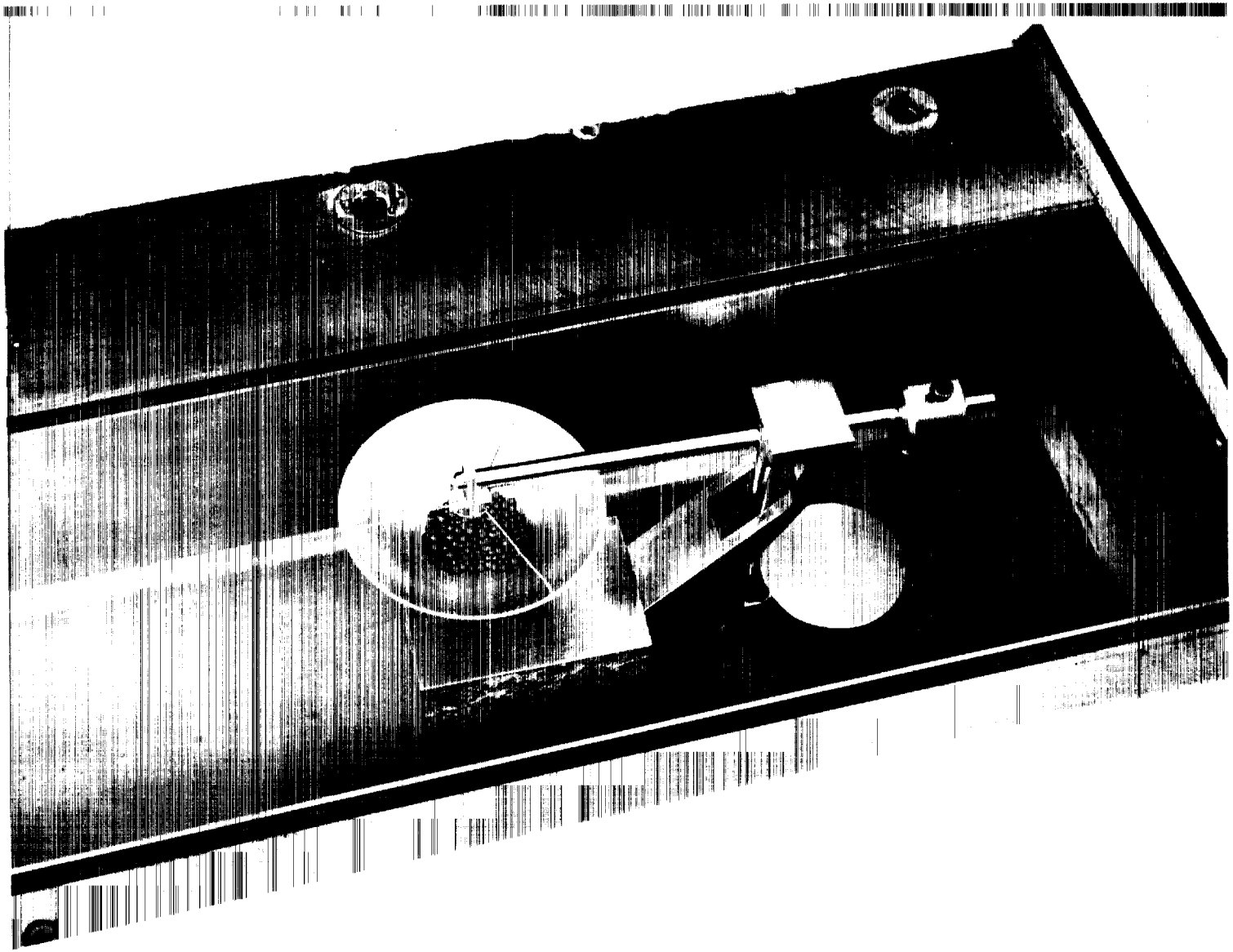

Figure 7. Calibration Fixture.

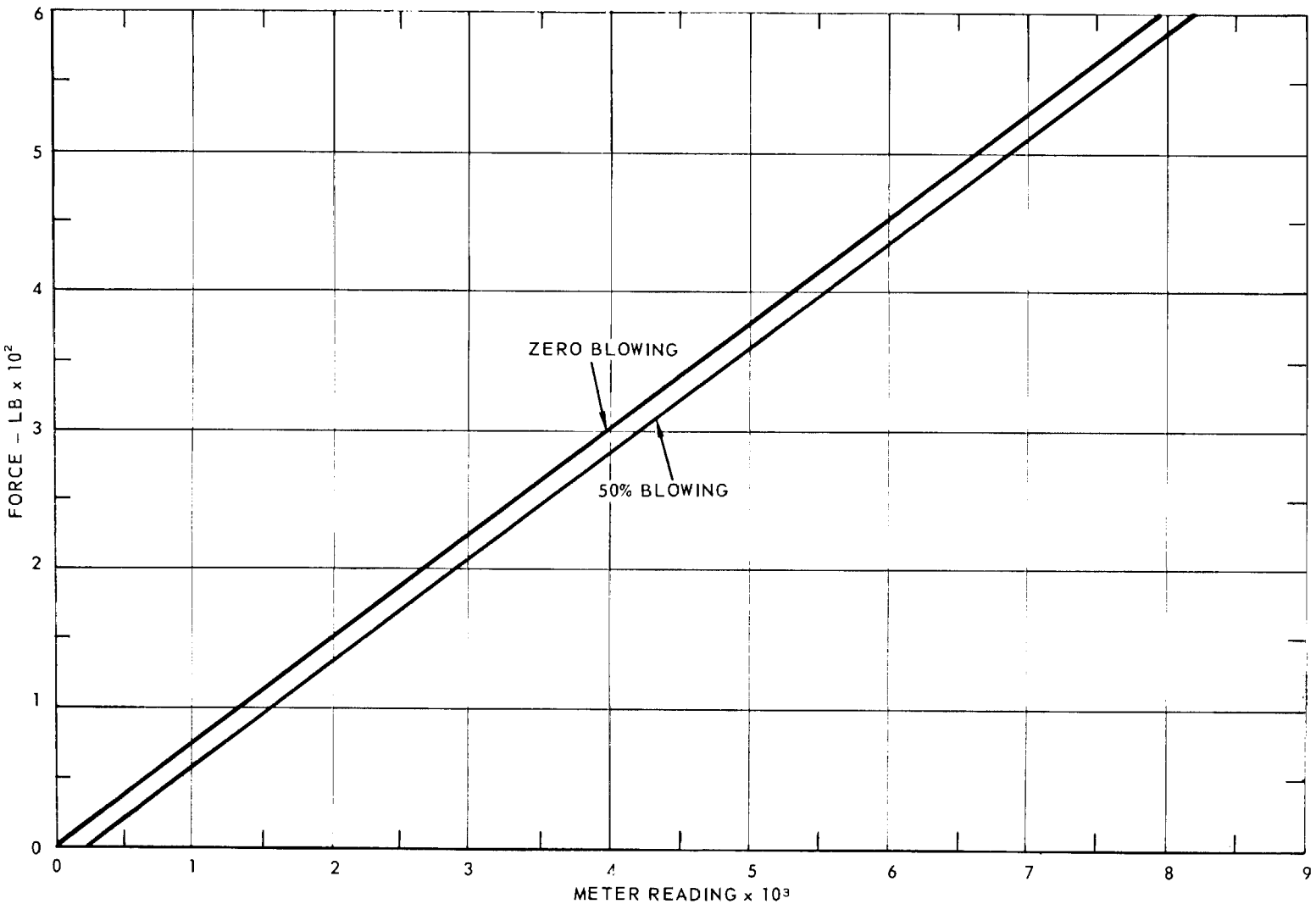

Figure 8. Typical Skin Friction Balance – Calibration Curves.

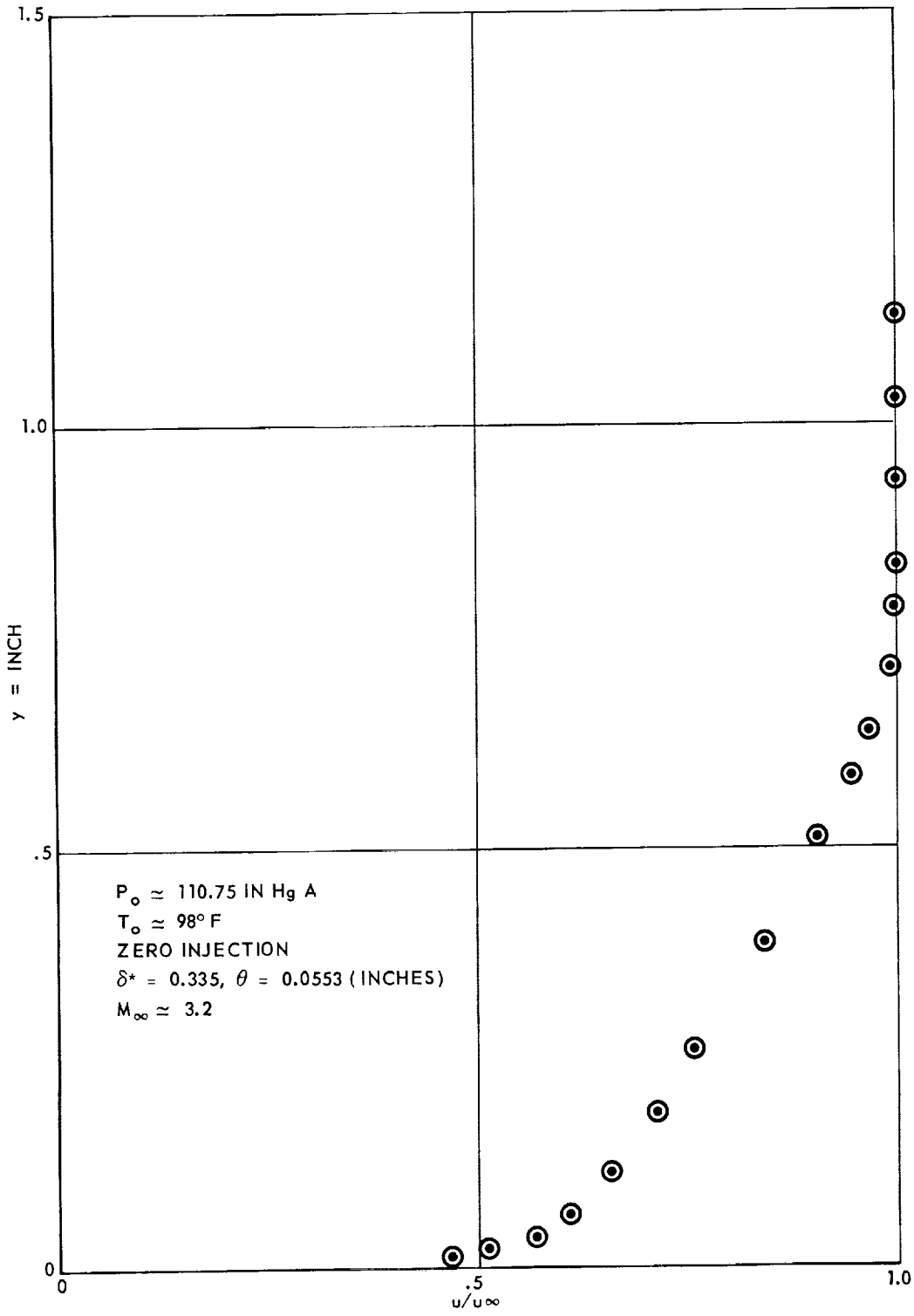

Figure 9A. Velocity Profiles Upstream of Balance.

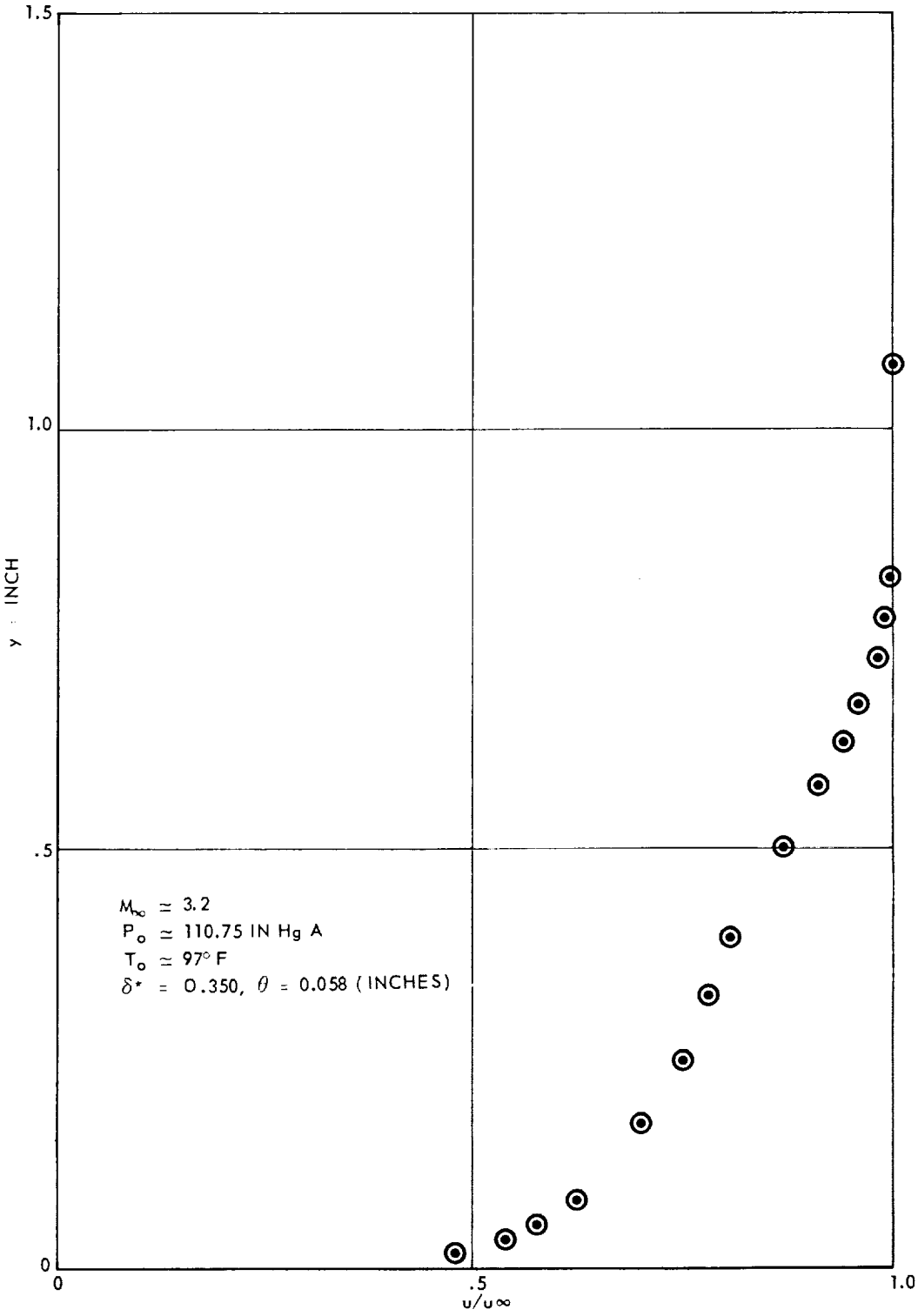

Figure 9B. Velocity Profiles Over Balance.

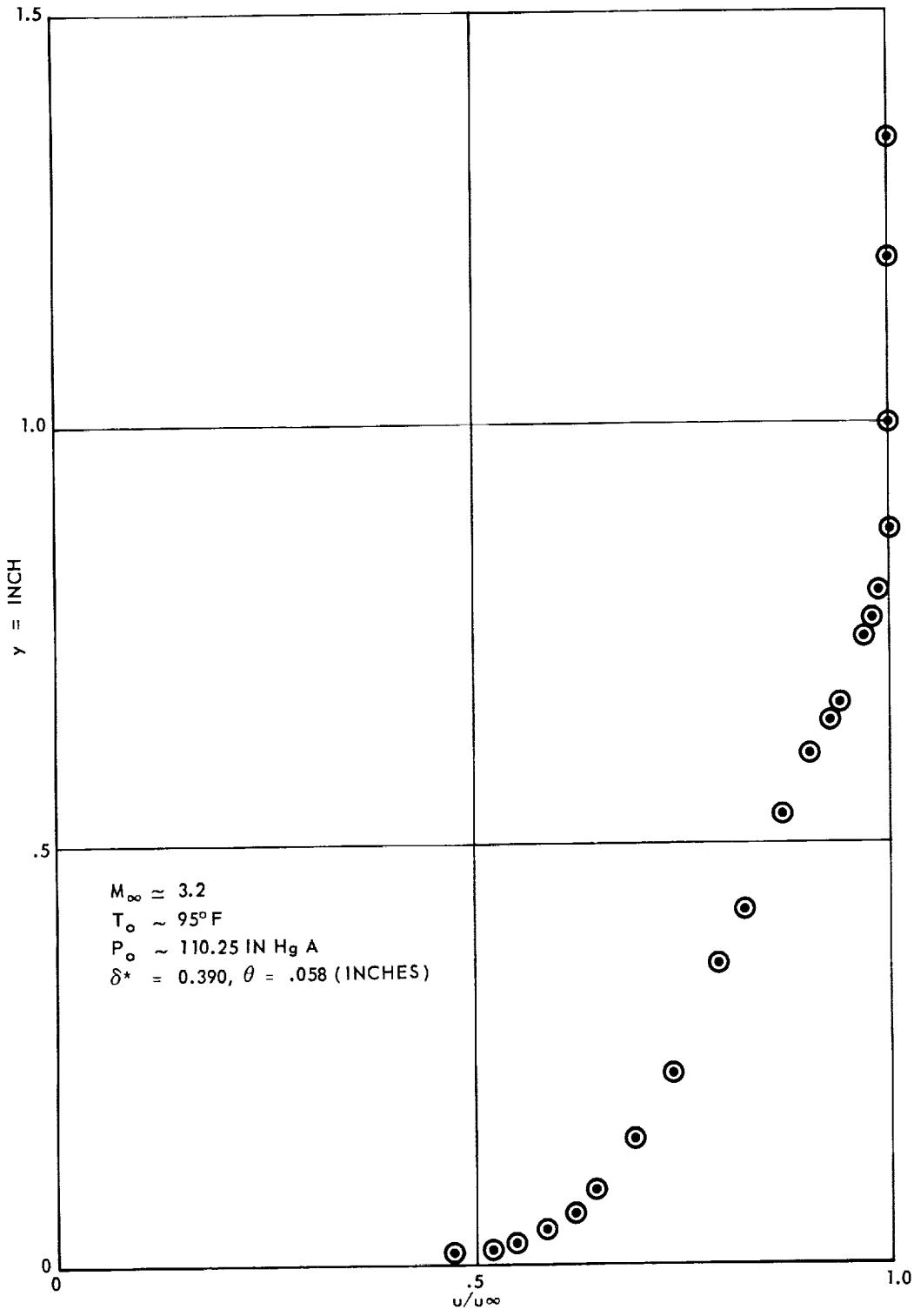

Figure 9C. Velocity Profiles Downstream of Balance.

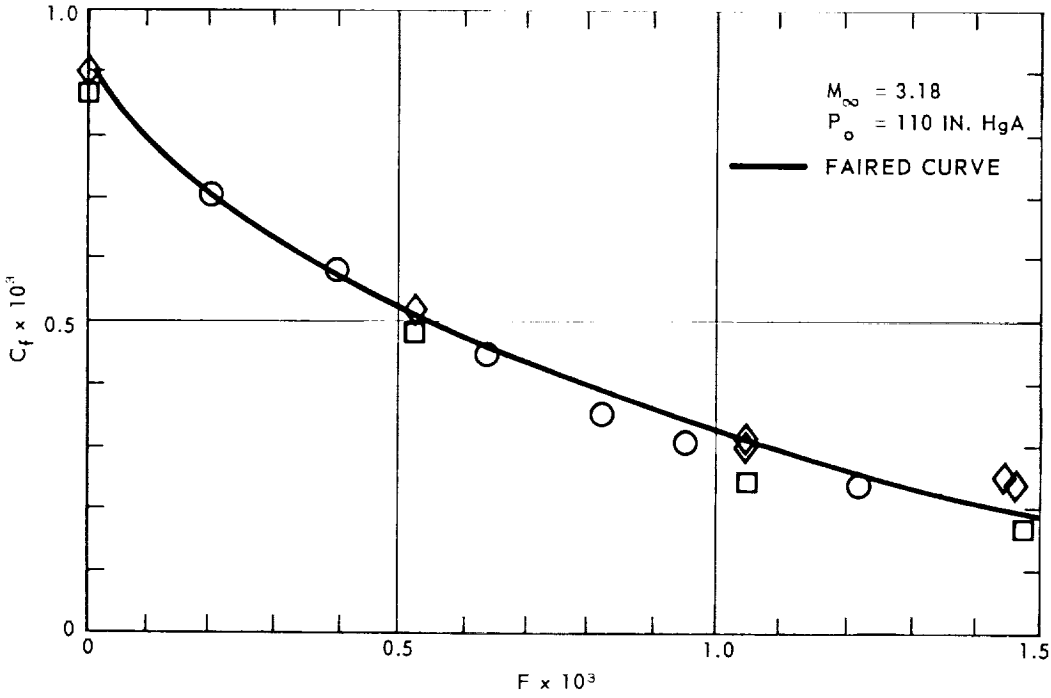

Figure 10. Skin Friction Coefficient Versus Blowing Ratio.

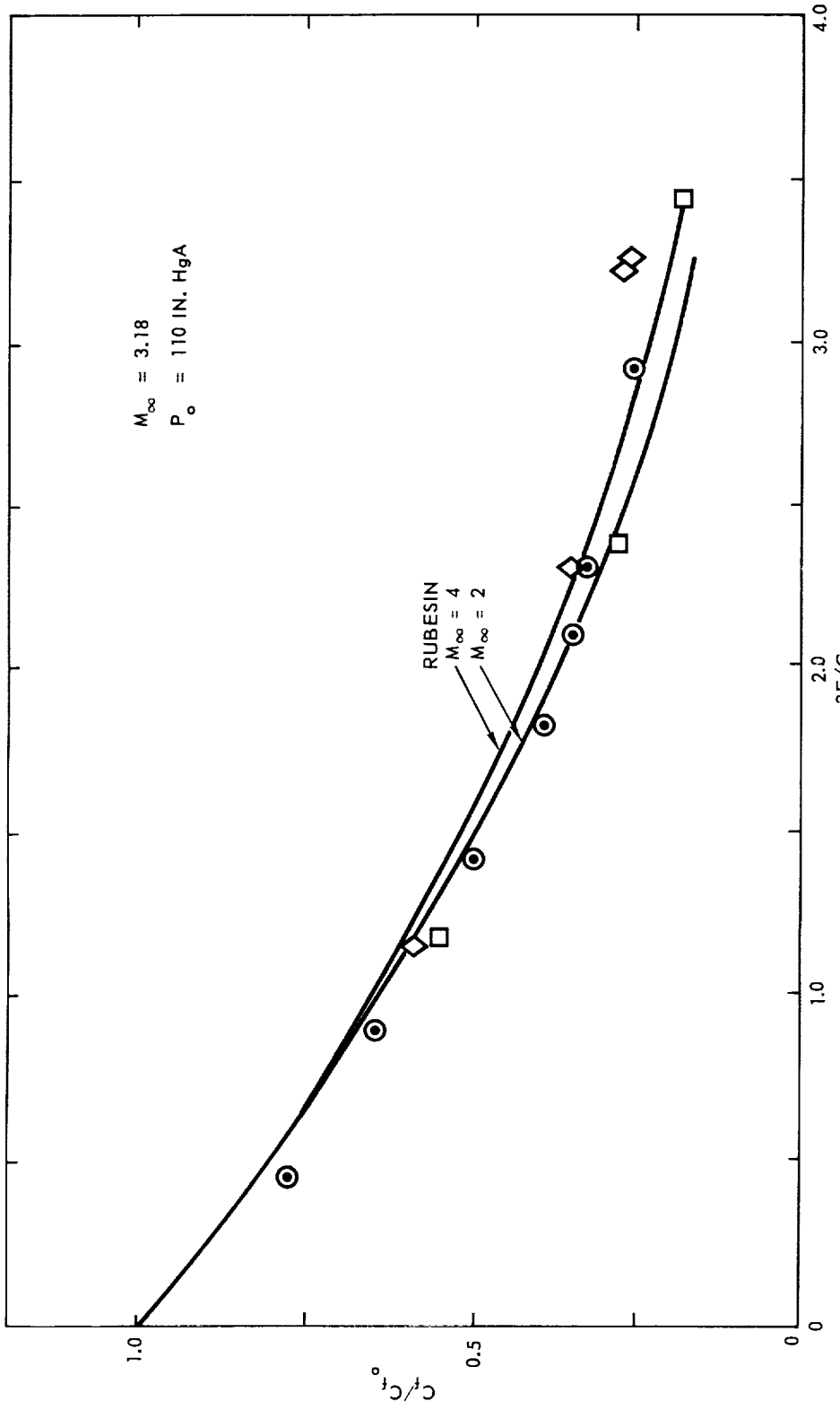

Figure 11. Skin Friction Ratio Versus Blowing Parameter $2F/C_{f_o}$.

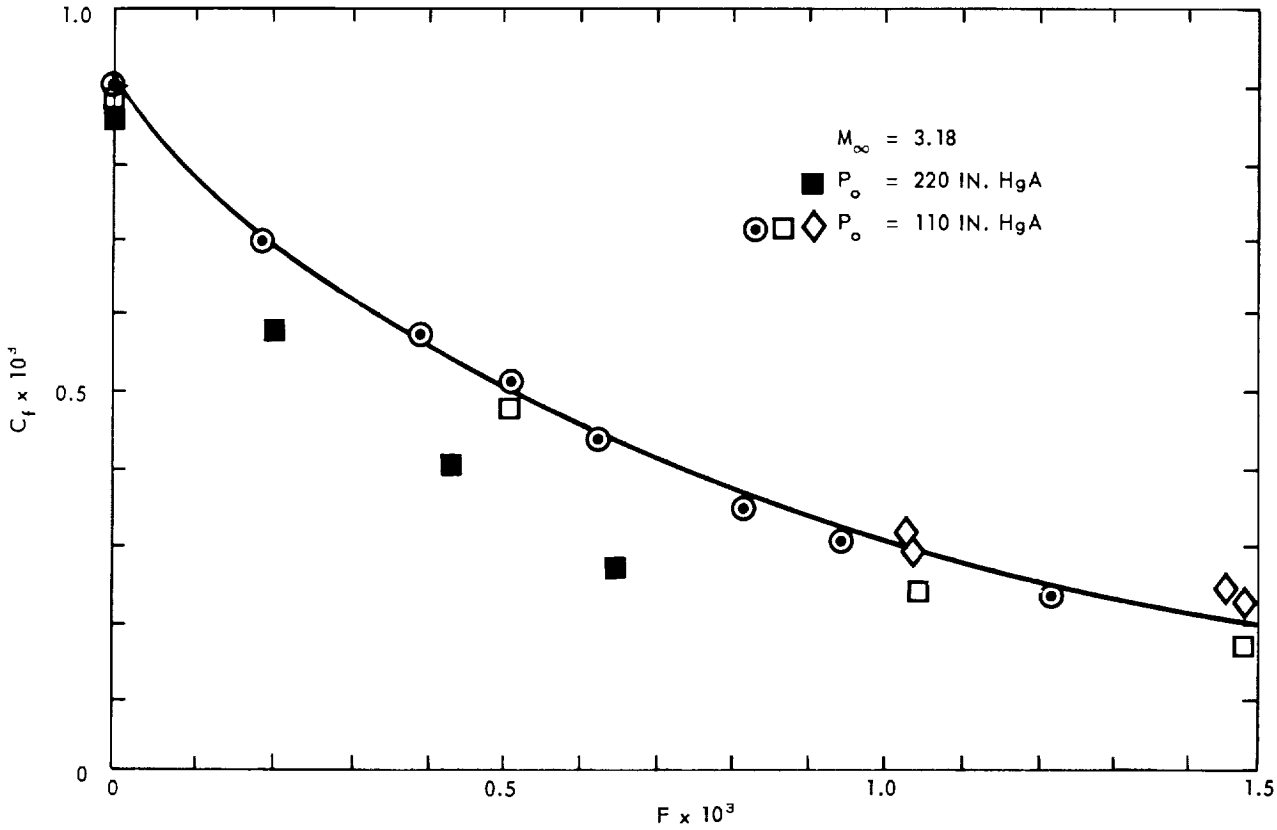

Figure 12. Skin Friction Coefficient Versus Blowing Ratio.

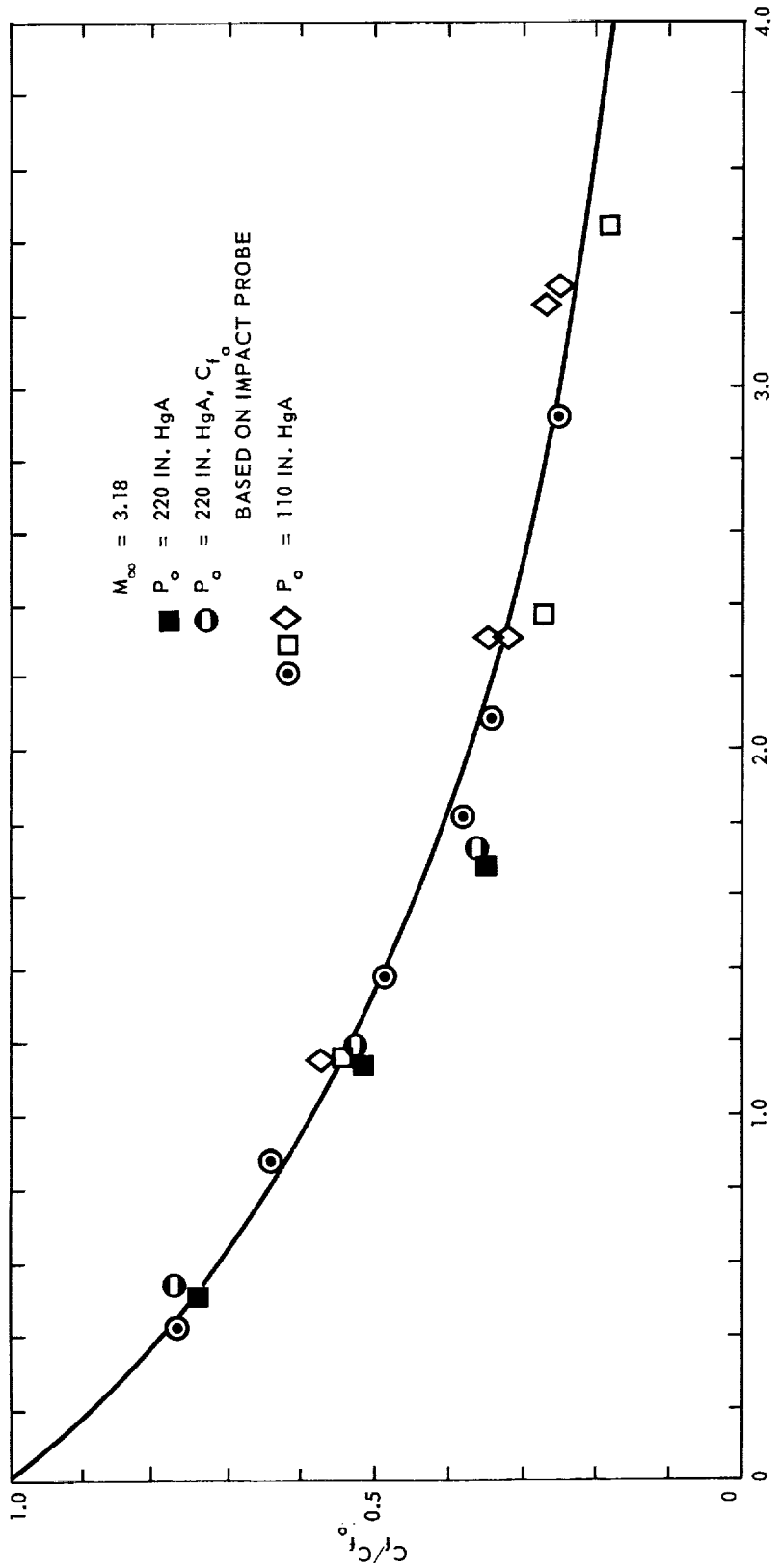

Figure 13. Skin Friction Ratio Versus Blowing Parameter.

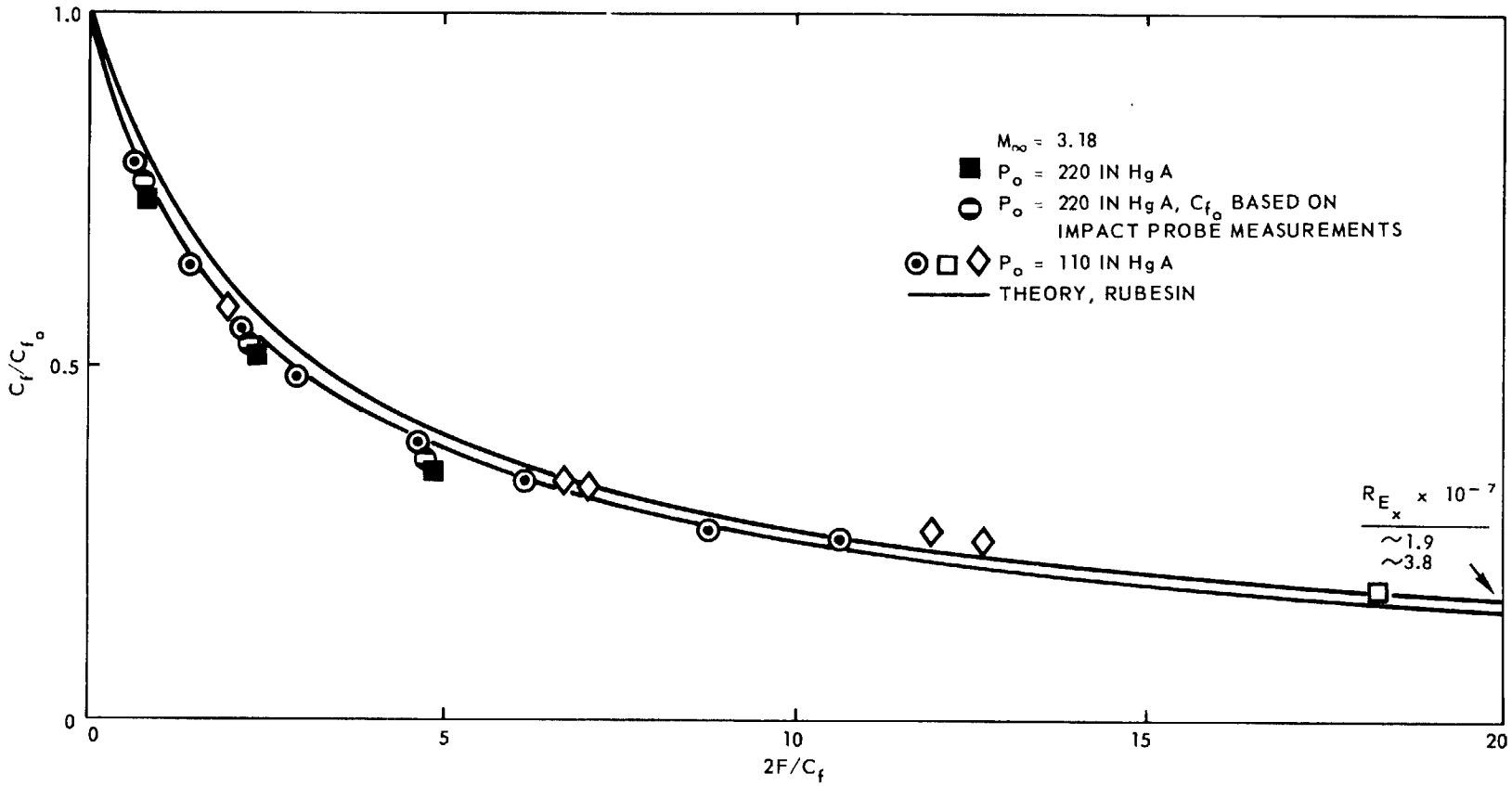

Figure 14. Skin Friction Ratio Versus Blowing Parameters $2F/C_f$.

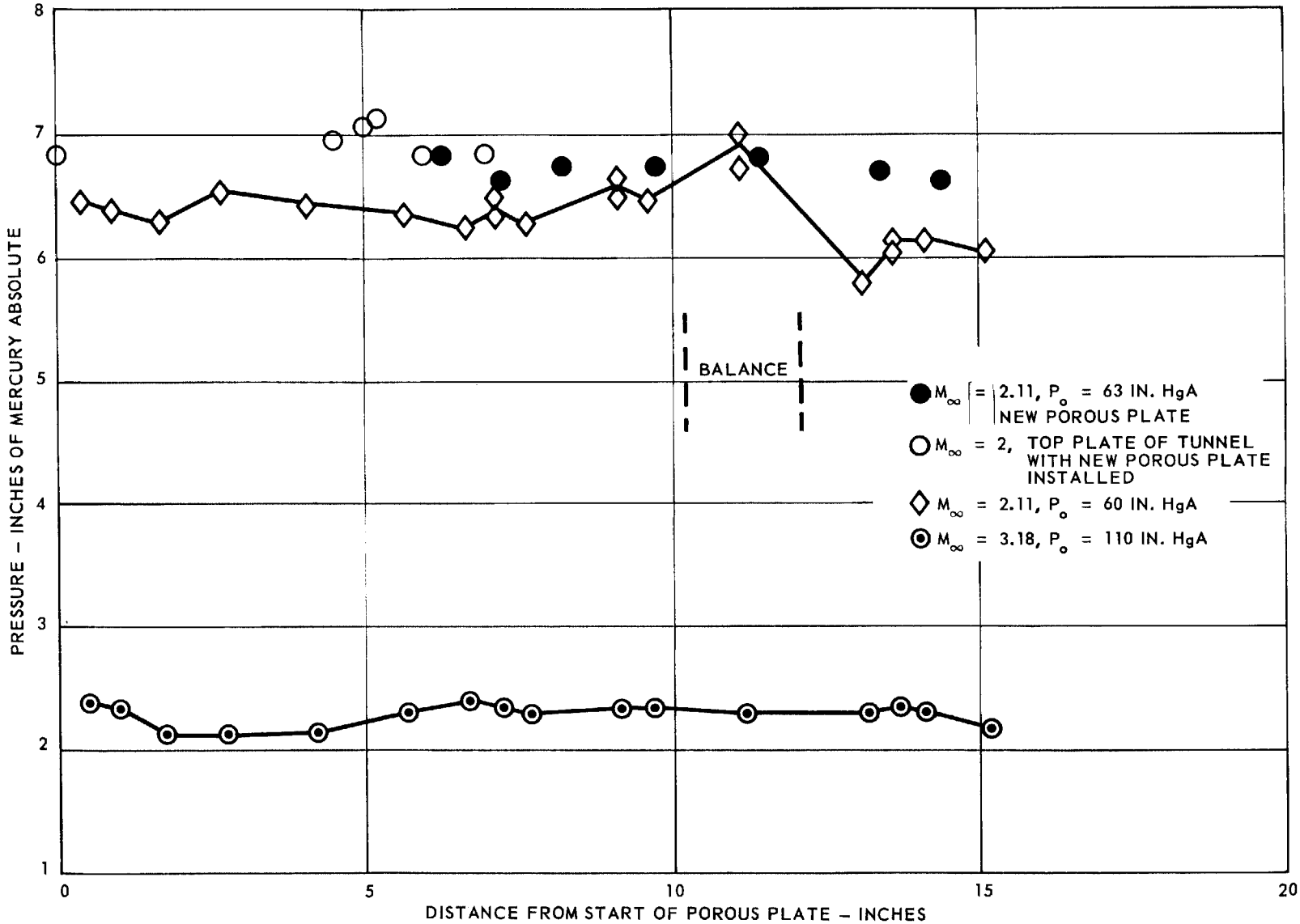

Figure 15. Pressure Distribution on Porous Plate.

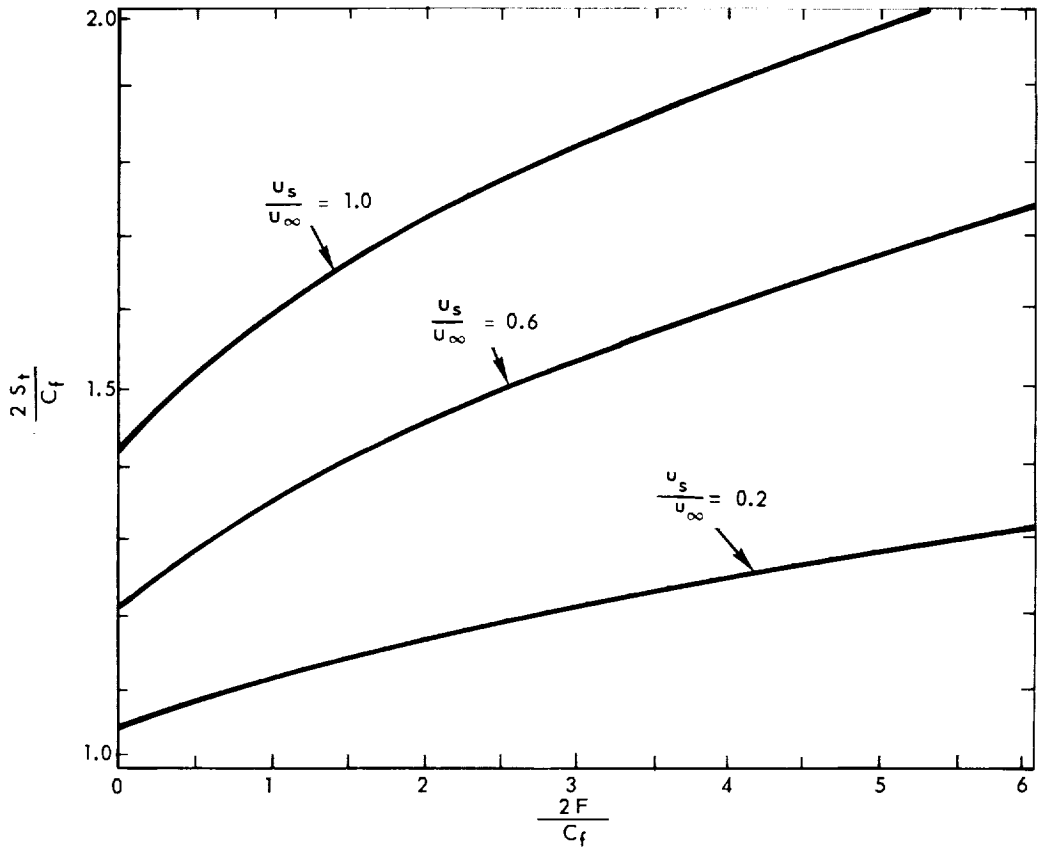

Figure 16. Reynolds Analogy for Mass Transfer – Dorrance.

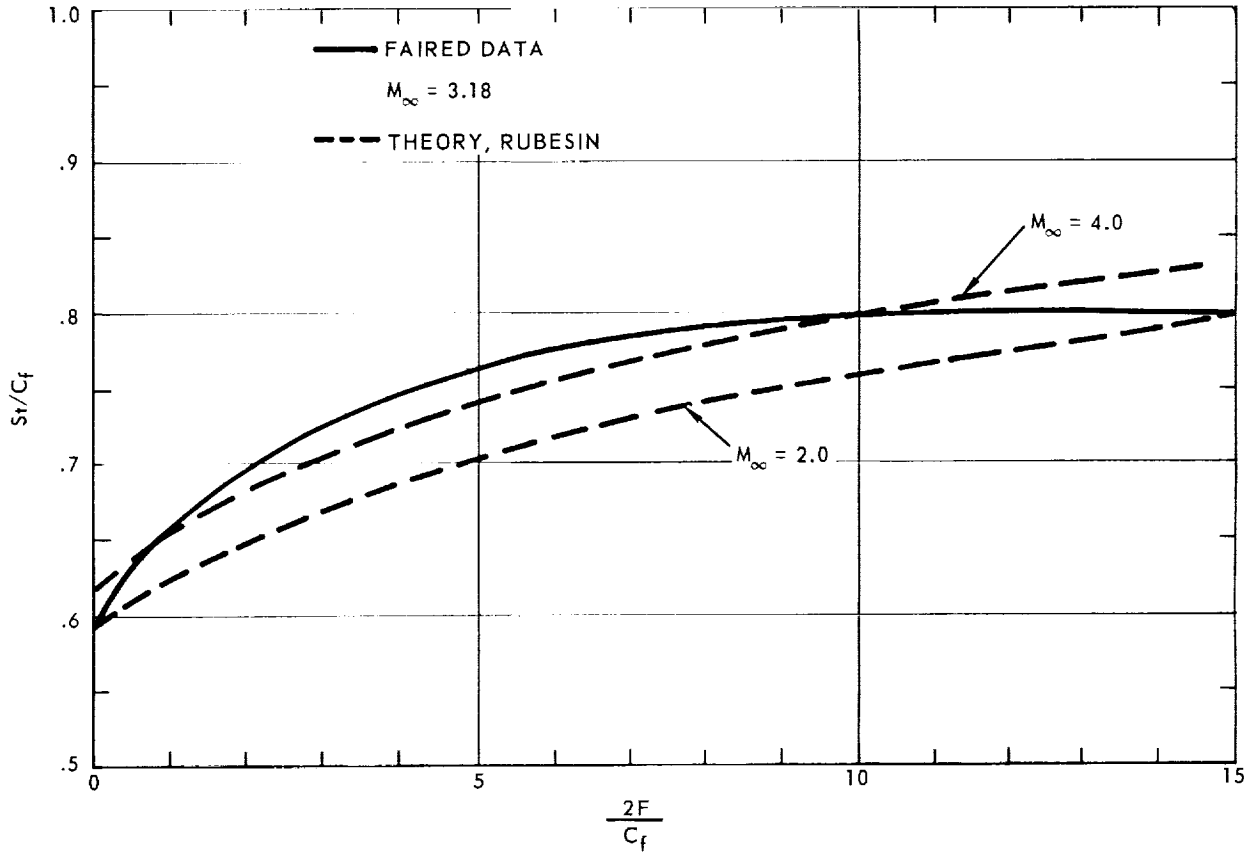

Figure 17. Reynolds Analogy for Mass Transfer.

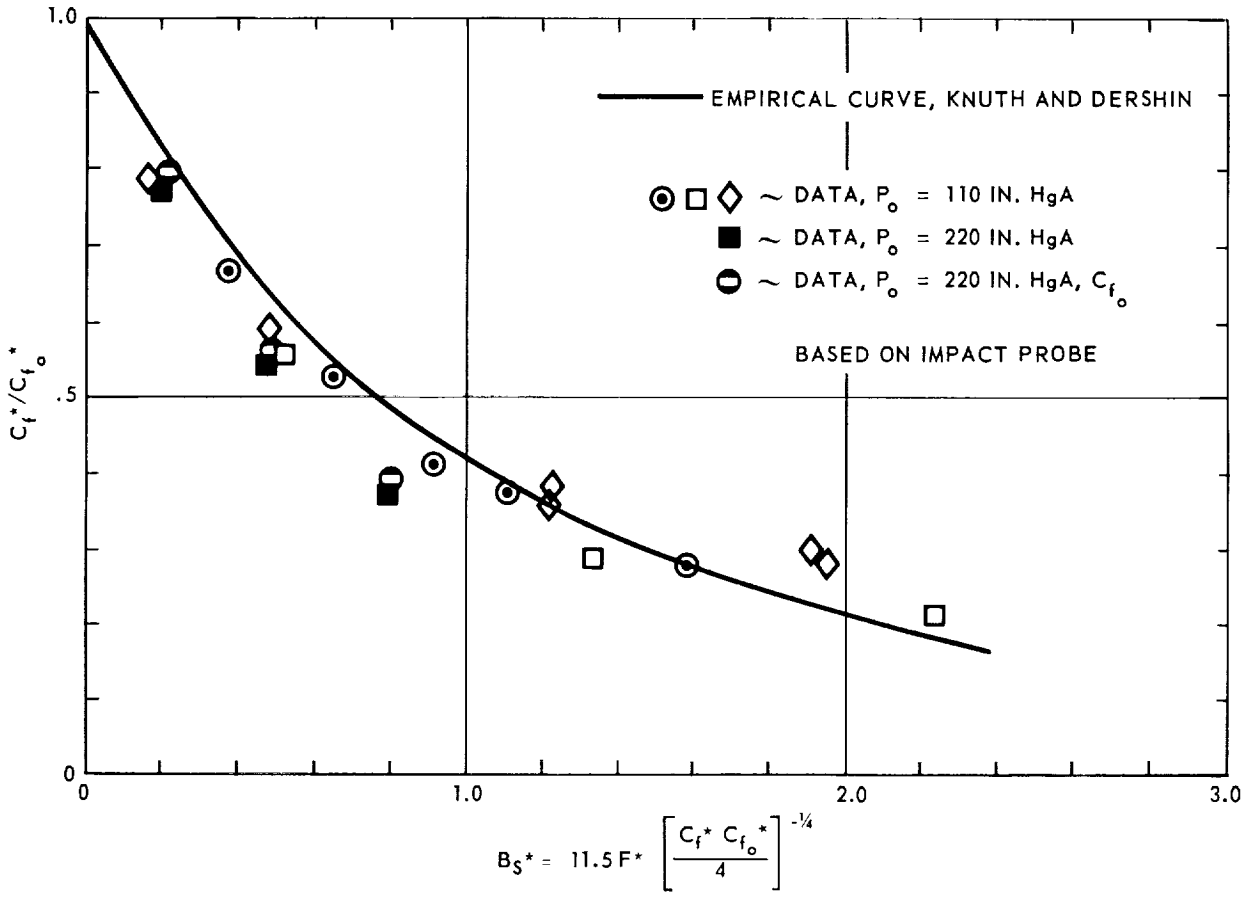

Figure 18. Skin Friction Ratio Versus Blowing Parameter – Reference Temperature Plane.

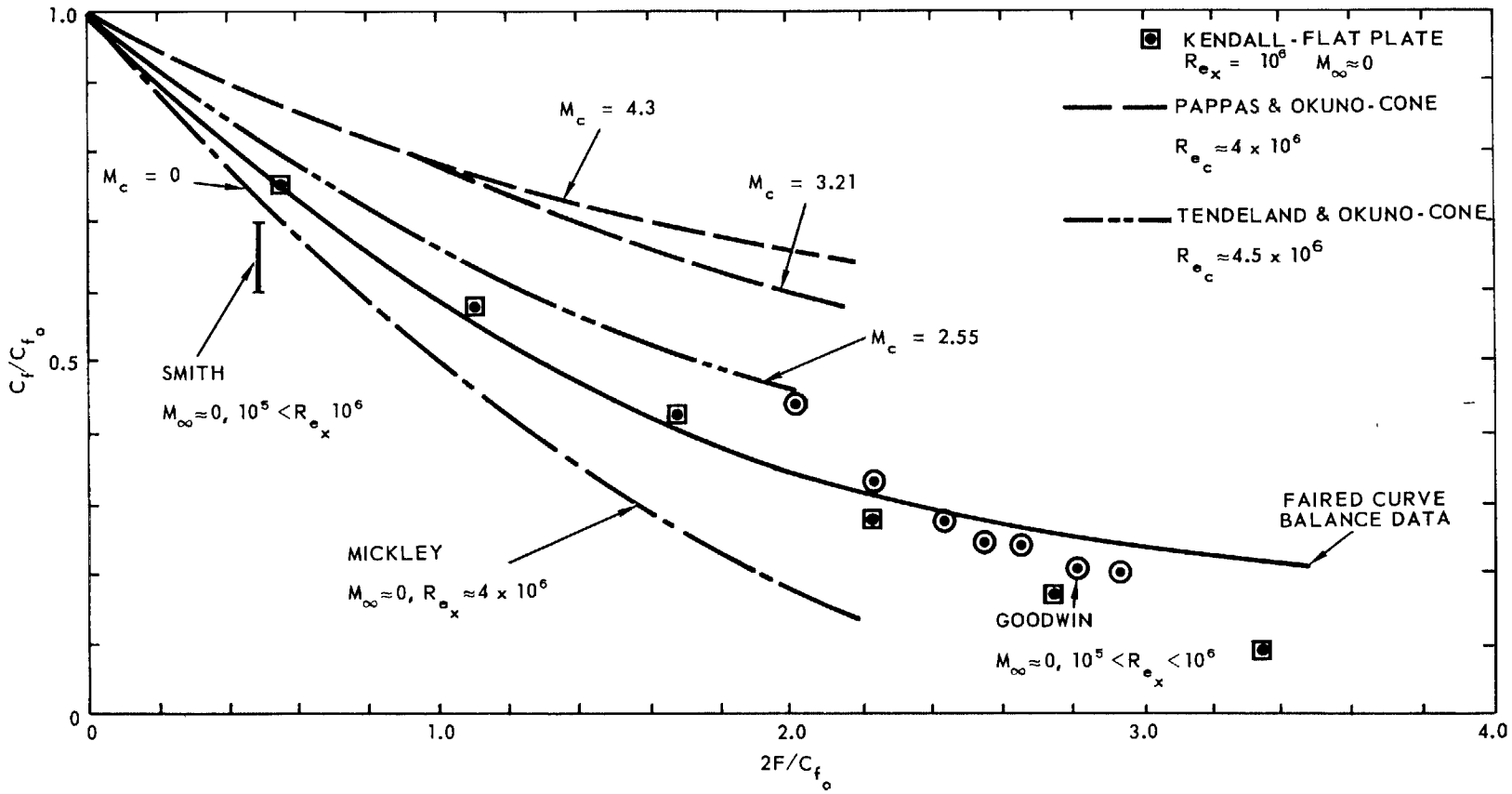

Figure 19. Comparison of Skin Friction Data.